Available online at www.sciencedirect.com
SCIENCE DIRECT®
Journal of Organometallic Chemistry 690 (2005) 3803–3814
Journal of Organometallic Chemistry
www.elsevier.com/locate/jorganchem

Synthesis, characterization, reactivity and theoretical studies of ruthenium carbonyl complexes containing *ortho*-substituted triphenyl phosphanes

M. Andreina Moreno [a], Matti Haukka [a,*], Sirpa Jääskeläinen [a], Sauli Vuoti [b], Jouni Pursiainen [b], Tapani. A. Pakkanen [a]

[a] *Department of Chemistry, University of Joensuu, P.O. Box 111, FI-80101, Joensuu, Finland*
[b] *Department of Chemistry, University of Oulu, P.O. Box 3000, FI-90014,Oulu, Finland*

Received 6 March 2005; received in revised form 10 May 2005; accepted 11 May 2005
Available online 20 June 2005

Abstract

A series of ruthenium *o*-phosphane complexes was synthesized and characterized. The reactivity of the prepared complexes was studied by using them as catalysts for the hydroformylation of 1-hexene. The activities depended on the binding mode of the phosphane and on the strength of the ruthenium–phosphane interaction. Strongly coordinated chelating [2-(dimethylamino)phenyl]-(diphenyl) phosphane and [2-(methylthio)phenyl]-(diphenyl) phosphane showed poor activity, while weakly chelated [2-(methoxy)phenyl]-(diphenyl) phosphane and non-chelating phosphanes such as [2-(methyl)phenyl]-(diphenyl) phosphane or [2-(ethyl)phenyl]-(diphenyl) phosphane led to higher activities.

Keywords: Ruthenium; Phosphanes; Hydroformylation

1. Introduction

Phosphanes are widely used ligands in complex chemistry because of the variety of properties they exhibit. They can stabilize charge on a metal centre [1,2], generate vacancies for coordination [3,4], or favour a specific geometrical configuration in a metal complex providing high catalytic selectivity towards specific products [5]. They can also act as pro-chiral ligands helping in the obtaining of chiral products for pharmaceutical applications [6]. Among different phosphanes, those containing coordinating subtituents in the *ortho*-position display useful properties. If the substituents can switch between coordinated and uncoordinated mode they can be considered as hemilabile ligands. Substitution in the *ortho* position permits an efficient charge donation from ligand to metal and favours chelation, but it also introduces higher steric requirements. Thus, the overall effect varies according to the nature of the *ortho* substituent.

Extensive work has been devoted to the development of new phosphane ligands and the corresponding metal complexes in order to tailor the catalytic properties. Ruthenium compounds with phosphane ligands are known to have applications in various fields of catalysis, including hydrogenation [7–9], isomerization [10–14] and hydroformylation reactions [15–18]. Although ruthenium–phosphanes are well-known systems, they are still of interest. Studies on new ruthenium complexes [19] as well as mechanistic reports [20,21] on catalytic behaviour have been recently published. Furthermore, properties such as hemilability have been exploited in

* Corresponding author. Tel.: +358 13 251 3346; fax: +358 13 251 3344.
E-mail address: Matti.Haukka@joensuu.fi (M. Haukka).

0022-328X/$ - see front matter © 2005 Elsevier B.V. All rights reserved.
doi:10.1016/j.jorganchem.2005.05.016

other applications, for example in the development of sensors [22] or as a tool in supramolecular chemistry [23].

In this study, we report on the preparation and characterization of a series of ruthenium carbonyl complexes containing *ortho*-substituted phosphane ligands. The chemical reactivity of the complexes is studied by using 1-hexene hydroformylation as a probe reaction. The formation of the new complexes is further investigated by means of computational DFT calculations as well as spectroscopic and crystallographic analysis. The steric factors of the phosphane ligands are considered from the point of view of cone angles. The chelation effects of the bidentate phosphanes over the reactivity of the coordinated complexes are also discussed. Schematic pictures of the studied phosphanes are shown in Fig. 1.

2. Experimental

FT-IR measurements were performed on a Nicolet Magna 750 spectrometer. ^{31}P NMR of the metal complexes was recorded on a Bruker Avance with a resonance frequency of 250 MHz. Elemental analysis of the complexes was done on EA1110 CHNS-O equipment (CE instruments). All reactions were performed under nitrogen, and the solvents were also degassed prior to use. Crystals were obtained by recrystallization from a mixture 1:1 of hexane and dichloromethane.

2.1. Synthetic procedure: chelated complexes

$[RuCl_2(CO)_3]_2$ (200 mg, 0,39 mmol) and 120 mg of the correspondent ligand op = [2-(methoxy)phenyl]-(diphenyl) phosphane (0.78 mmol), sp = [2-(methylthio)phenyl]-(diphenyl) phosphane (0.41 mmol) or np = [2-(dimethylamino)phenyl]-(diphenyl) phosphane (0.39 mmols) diphenylphosphane were dissolved in separated flasks in 4 ml of degassed ethanol. The solutions were combined and stirred overnight. A white solid precipitate was formed. The solid was filtered, washed with ethanol, and dried under vacuum. The chelated (op) complex $[RuCl_2(CO)(\eta^2\text{-op})(op)]$ **3** was obtained in a similar way as described by Jeffrey and Rauchfuss [24]. Irradiation of a sample of $[RuCl_2(CO)_2(op)_2]$ **4** dissolved in CH_2Cl_2 with UV light for 8 h, yields complex **3** when the solvent was removed by means of a vacuum, colourless crystals of **3** were formed.

2.1.1. Characterization

(OC-6-42)$[RuCl_2(CO)_2(\eta^2\text{-np})]$ (**1**); np = [2-(dimethylamino)phenyl]-(diphenyl) phosphane. ν(CO) = 2006, 2069 cm^{-1} in CH_2Cl_2, δ_P ($CDCl_3$) 49.1s. Anal. Calc. for **1**: H, 3.78; C, 49.54; N, 2.63. Found: H, 3.78; C, 49.31; N 2.62%. Yield = 85%.

(OC-6-43)$[RuCl_2(CO)_2(\eta^2\text{-sp})]$ (**2**); sp = [2-(methylthio)phenyl]-(diphenyl) phosphane. ν(CO) = 2016, 2075 cm^{-1} in KBr pellets, δ_P ($CDCl_3$) 55.6s. Anal. Calc. for **2**: H, 3.28; C, 47.03. Found: H, 3.28; C, 47.04%. Yield = 88%.

(OC-6-12)$[RuCl_2(CO)(\eta^2\text{-op})(op)]$ (**3**); op = [2-(methoxy)phenyl]-(diphenyl) phosphane. ν(CO) = 1968 cm^{-1} (in CH_2Cl_2), δ_P ($CDCl_3$) 34.0s. Anal. Calc. for **3**: H, 3.22; C, 47.32. Found: H, 3.22; C, 47.17%. Yield = 65%.

2.2. Synthetic procedure: non-chelated complexes

$[RuCl_2(CO)_3]_2$ (200 mg, 0.39 mmol) and 228 mg (0.83 mmol) of [2-(methyl)phenyl]-(diphenyl) phosphane, (0.79 mmol) of bis[2-(methyl)phenyl]-(phenyl) phosphane, (0.79 mmol) of [2-(ethyl)phenyl]-(diphenyl) phosphane, (0.72 mmol) of bis[2-(ethyl)phenyl]-(phenyl) phosphane, (0.87 mmol) of triphenylphosphane, and (0.78 mmol) of [2-(methoxy)phenyl]-(diphenyl) phosphane were

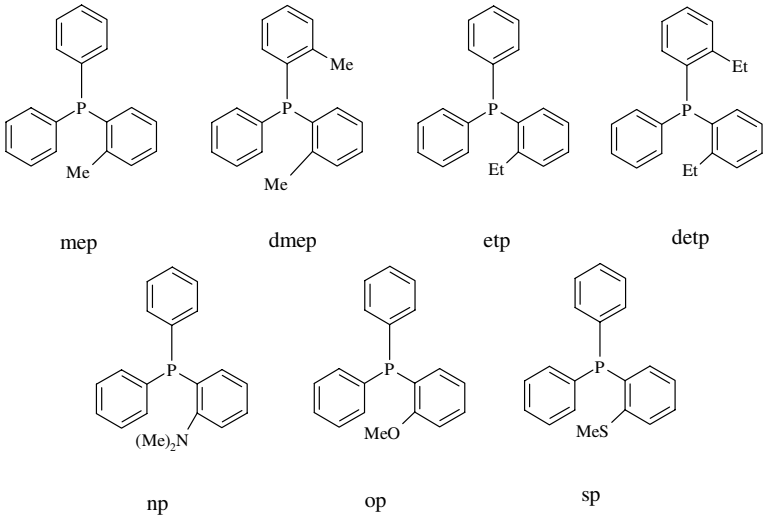

Fig. 1. Schematic structures of the ligands under study.

dissolved in separated flasks in 4 ml of degassed ethanol. The solutions were combined and stirred overnight (18 h). A white-yellowish solid precipitate was formed. The solid was filtered, washed with ethanol, and dried under vacuum.

2.2.1. Characterization

(OC-6-33)[$RuCl_2(CO)_2(op)_2$] (**4**); op = [2-(methoxy)phenyl]-(diphenyl) phosphane. ν(CO) = 1994, 2059 cm^{-1} in KBr pellets, δ_P ($CDCl_3$) 10.6s. Anal. Calc. for **4**: H, 4.48; C, 56.55. Found: H, 4.35; C, 56.29%. Yield = 95%.

(OC-6-33)[$RuCl_2(CO)_2(pph_3)_2$] (**5**); pph_3 = triphenylphosphane. ν(CO) = 1992, 2055 cm^{-1} for the (OC-6-33) isomer and 2016.5, 2080.6 cm^{-1} for the (OC-6-12) isomer in KBr pellets, δ_P ($CDCl_3$) 17.5s. Anal. Calc. for **5**: C, 54.31, H, 3.92. Found: C, 53.8; H, 3.54%. The characterization data is in good agreement with that reported by Batista et al. [25].

(OC-6-33)[$RuCl_2(CO)_2(mep)_2$] (**6**); mep = [2-(methyl)phenyl]-(diphenyl) phosphane. For the (OC-6-33) isomer: ν(CO) = 1978, 2046 cm^{-1} in KBr pellets, δ_P ($CDCl_3$) 16.2s. Anal. Calc. for **6**: H, 4.32; C, 59.89. Found: H, 4.28; C, 59.63%. Yield = 85%. FT-IR (CH_2Cl_2) also shows another dicarbonyl isomer located at 2075 and 2143 cm^{-1} presumably the (OC-6-12) isomer.

(OC-6-33)[$RuCl_2(CO)_2(dmep)_2$] (**7**); dmep = bis[2-(methyl)phenyl]-(phenyl) phosphane. ν(CO) = 1990, 2052 cm^{-1} in KBr pellets, δ_P ($CDCl_3$) 14.5s. Anal. Calc. for **7**: H, 4.74; C, 62.38. Found: H, 4.72; C, 61.56%. Yield = 87%.

(OC-6-33)[$RuCl_2(CO)_2(etp)_2$] (**8**); etp = [2-(ethyl)phenyl]-(diphenyl) phosphane. ν(CO) = 2012, 2073 for the (OC-6-33); and 1996, 2058 cm^{-1} for the (OC-6-12) isomer in CH_2Cl_2, δ_P ($CDCl_3$) 15.6s. Anal. Calc. for **8**: H, 4.33; C, 54.01. Found: H, 4.32; C, 53.86%. Yield = 92%.

[$Ru(\mu\text{-}Cl)Cl(CO)_2(detp)]_2$ (**9**); detp = bis[2-(ethyl)phenyl]-(phenyl) phosphane. ν(CO) = 2011, 2071 cm^{-1} in CH_2Cl_2, δ_P ($CDCl_3$) 36.1s. Anal. Calc. for **9**: C, 52.76; H, 4.24. Found: C, 52.61; H, 4.39%. Solid precipitates after a week and with stirring at room temperature. Yield = 65%.

2.3. Catalysis

The hydroformylation reactions were performed in high-pressure autoclaves (100 ml Berghof) equipped with a teflon liner. The autoclaves were charged in a glove box. In a typical experiment, the solvent 1-methyl-2-pyrrolidinone (5 ml), the standard cyclohexane (0.2 ml), the olefin 1-hexene (0.5 ml), and the catalyst were added to the autoclave, which was then pressurized to 20 bar with synthesis gas CO/H_2 1:1. The autoclave was heated at 120 °C for 17 h. The reaction was then stopped and the autoclave was rapidly cooled to room temperature and brought to atmospheric pressure, after which the liquid samples were analysed. The product distribution is reported as wt%.

The gases CO and H_2 used in the hydroformylation experiments were of 99% and 99.99% purity, respectively. The solvent 1-methyl-2-pyrrolidone (Aldrich 99%) and the internal standard cyclohexane (Merck 99%) were used without further purification and degassed with nitrogen before use. Similarly, 1-hexene (99%) was degassed prior to use. Gas chromatographic analyses of the product mixture were recorded on a Hewlett–Packard 5890 series II chromatograph equipped with a Varian WCOT fused silica 50 M × 0.53 M column and temperature programming.

2.4. X-ray structure determinations

The X-ray diffraction data was collected using a Nonius KappaCCD diffractometer using Mo Kα radiation (λ = 0.71073 Å). Single crystals of **1**–**4** and **6**–**9** were mounted in inert oil to the cold gas stream of the diffractometer. The Denzo-Scalepack [26] program package was used for cell refinements and data reduction. The structures were solved by direct methods using the SHELXS-97 or SIR-2002 programs [27,28]. A multiscan absorption correction based on equivalent reflections (XPREP in SHELXTL v. 6.14) [29] was applied to all data (T_{min}/T_{max}) values were 0.29924/0.36289, 0.30170/0.35219, 0.14144/0.19398, 0.24387/0.31003, 0.24317/0.29114 for **1**–**4** and 0.14979/0.19128, 0.23453/0.30346, and 0.24387/0.31003, respectively, for **6**–**9**. All structures were refined with SHELXL-97 [30] and WinGX graphical user interface [31]. In **4** the phenyl ring containing OMe group and one of the plain phenyl rings were disordered over two sites with occupancies of 0.62:0.48. Due to the disorder both rings were refined with fixed C–C distances of 1.390 Å. Furthermore, the carbons C5A and C5B were refined with equal anisotropic displacement parameters. In **6** one of the methyl groups was also disordered between two phenyl rings with occupancies of 0.64:0.36. All of the hydrogens were placed in an idealized position and constrained to ride on their parent atom. The crystallographic data is summarized in Table 1 and the selected bond lengths and angles in Table 2. Thermal ellipsoid plots of **1**, **2**, **3**, **6** and **9** are shown in Figs. 2–6. The plots of **4**, **7** and **8** are given as Supplementary material.

2.5. Computational details

The geometries of the complexes were optimized using the B3PW91 hybrid density functional method and employing 6-31G* as a basis set (for ruthenium: Huzinaga's extra basis 433321/4331/421) [32]. The geometry optimizations were followed by analytical frequency

Table 1
Crystallographic data for **1–4** and **6–9**

Complex	**1**	**2**	**3**	**4** · CH_2Cl_2	**6** · $2(CH_2Cl_2)$	**7** · $2(CH_2Cl_2)$	**8** · $2(CH_2Cl_2)$	**9**
Emperical formula	$C_{22}H_{20}Cl_2NO_2PRu$	$C_{21}H_{17}Cl_2O_2PRuS$	$C_{39}H_{34}Cl_2O_3P_2Ru$	$C_{41}H_{36}Cl_4O_4P_2Ru$	$C_{42}H_{38}Cl_6O_2P_2Ru$	$C_{44}H_{42}Cl_6O_2P_2Ru$	$C_{44}H_{42}Cl_6O_2P_2Ru$	$C_{50}H_{50}Cl_8O_4P_2Ru_2$
Formula weight	533.33	536.35	784.57	897.51	950.43	978.49	978.49	1262.58
T (K)	120(2)	120(2)	100(2)	120(2)	100(2)	120(2)	120(2)	120(2)
λ (Å)	0.71073	0.71073	0.71073	0.71073	0.71073	0.71073	0.71073	0.71073
Crystal system	Monoclinic	Monoclinic	Monoclinic	Monoclinic	Triclinic	Triclinic	Triclinic	Monoclinic
Space group	$P2_1$	$P2_1/n$	$P2_1/c$	$P2_1/n$	$P\bar{1}$	$P\bar{1}$	$P\bar{1}$	$P2_1/c$
a (Å)	9.6597(6)	12.5494(2)	10.1149(3)	10.2229(3)	10.0544(4)	10.3071(2)	10.0163(2)	13.2160(6)
b (Å)	10.9516(7)	10.9775(2)	21.0646(5)	31.0971(12)	13.5292(7)	14.0818(2)	14.2547(4)	10.7652(6)
c (Å)	10.8446(7)	16.1733(4)	16.3599(4)	12.7519(4)	15.4587(9)	15.2056(2)	15.1764(5)	18.8603(8)
α (°)	90	90	90	90	105.688(2)	106.5830(10)	78.071(1)	90
β (°)	106.435(4)	100.9950(10)	101.855(2)	101.082(2)	91.344(3)	90.2190(10)	87.493(2)	98.334(3)
γ (°)	90	90	90	90	95.731(3)	92.3770(10)	89.032(2)	90
V (Å^3)	1100.37(12)	2187.15(8)	3411.39(15)	3978.3(2)	2011.57(18)	2113.08(6)	2117.98(10)	2655.0(2)
Z	2	4	4	4	2	2	2	2
ρ_{calc} (Mg/m^3)	1.610	1.629	1.528	1.498	1.569	1.538	1.534	1.579
μ (Mo Kα) (mm^{-1})	1.046	1.144	0.748	0.784	0.905	0.864	0.862	1.074
R_1[a] ($I \geqslant \sigma$)	0.0300	0.0280	0.0360	0.0515	0.0583	0.0364	0.0360	0.0368
wR_2[b] ($I \geqslant \sigma$)	0.0696	0.0670	0.0869	0.0887	0.1378	0.0884	0.0736	0.0671

[a] $R_1 = \sum||F_o| - |F_d|/\sum|F_o|$.
[b] $wR_2 = [\sum[w(F_o^2 - F_c^2)^2]/\sum[w(F_o^2)^2]]^{1/2}$.

calculations to obtain the vibration spectra and stationary point of all compounds. The calculations were made using the GAUSSIAN-03 program package.

3. Results and discussion

Reactions between the ruthenium dimer $[RuCl_2(CO)_3]_2$ and the selected phosphanes yielded two types of complexes: chelated and non-chelated. The chelated complexes (np) **1** and (sp) **2** contained only one phosphane ligand, while the chelated (op) complex **3** contained two. In contrast, all the non-chelating complexes contained two phosphane ligands. The reactions are summarized in Scheme 1.

In a typical reaction, FT-IR revealed the formation of tricarbonyl complexes containing one non-chelating phosphane ligand as a minor side product in most of the reactions involving non-chelating phosphanes.

3.1. Catalytic studies

The catalytic activity of all of the complexes was tested in 1-hexene hydroformylation. The activities are reported in Table 3. We used catalysis to study the reactivity of the complexes. In the series of chelated phosphanes catalytic activity is a good indication of the hemilabile character of these ligands and chelate effects, and in the non-chelated series, catalysis allows studying electronic and steric effects associated with reactivity.

3.1.1. Chelated complexes

The most distinct feature is that the activities of the chelated compounds are, in general, lower than the activities of the non-chelated ones. This is due to the higher stability of the chelated complexes, which are less eager to participate in the catalytic reaction. When compared with each other, the activities of the chelated ruthenium phosphane complexes follow the order: Ru(op) > Ru(sp) > Ru(np). Thus, chelated ruthenium (np) (**1**, Fig. 2) is considered the most stable complex because it is not active under catalytic conditions. The (np) ligand coordinates strongly through both nitrogen and phosphorus, resulting in a highly stable structure. The tendency to produce strongly chelated complexes is typical of this particular (np) ligand [33,34] and examples of non-chelated metal complexes of this ligand are, to the best of our knowledge, not reported. In contrast, other (np) ligands such as the 2-(diphenylphosphino)-pyridine (PPh_2py) [35–37] and the 2-(diphenylphosphino)-1-methyl-imidazole (dpim) [38] show slightly better hemilabile properties and the non-chelated metal complexes containing these phosphanes have been identified. In the latter two cases chelation has to be promoted in contrast to our complex in which the chelated product is the only one observed. The general problem with substi-

Table 2
Selected bond lengths (Å) and bond angles (°) for **1**–**4** and **6**–**9**

Complex	**1**	**2**	**3**	**4** · CH_2Cl_2	**6** · 2(CH_2Cl_2)	**7** · 2(CH_2Cl_2)	**8** · 2(CH_2Cl_2)	**9**
Ru(1)–Cl(1)	2.4065(9)	2.4397(6)	2.4072(7)	2.4525(13)	2.448(2)	2.4646(7)	2.4368(7)	2.4663(7)
Ru(1)–Cl(1A)								2.4648(7)
Ru(1)–Cl(2)	2.4597(9)	2.4023(7)	2.3667(8)	2.4362(12)	2.441(2)	2.4335(6)	2.4550(7)	2.3942(7)
Ru(1)–P(1)	2.2918(9)	2.3003(5)	2.3336(8)	2.4133(14)	2.424(2)	2.4549(6)	2.4327(7)	2.3768(8)
Ru(1)–P(2)			2.4232(8)	2.4136(14)	2.432(2)	2.4564(6)	2.4220(7)	
Ru(1)–C(1)	1.875(4)	1.914(3)	1.811(3)	1.860(6)	1.951(10)	1.893(3)	1.876(3)	1.864(3)
Ru(1)–C(2)	1.871(4)	1.876(3)		1.874(5)	1.874(8)	1.870(3)	1.931(4)	1.877(3)
Ru(1)–O(2)			2.263(2)					
Ru(1)–S(1)		2.4007(6)						
Ru(1)–N(1)	2.262(3)							
Cl(1)–Ru(1)–Cl(2)	89.85(12)	89.28(3)	93.51(10)	95.76(4)	90.0(2)	97.66(2)	96.63(2)	87.85(3)
C(1)–Ru(1)–C(2)	90.34(16)	91.46(11)		82.72(15)	90.7(3)	93.23(11)	92.18(11)	90.11(12)
C(1)–Ru(1)–O(2)			171.32(11)					
P(1)–Ru(1)–P(2)			177.09(3)	176.57(5)	176.56(6)	176.27(2)	175.93(3)	
P(1)–Ru(1)–S(1)		85.228(18)						
P(1)–Ru(1)–N(1)	81.14(7)							
Ru(1)–Cl(1)–Ru(1A)								98.89(2)

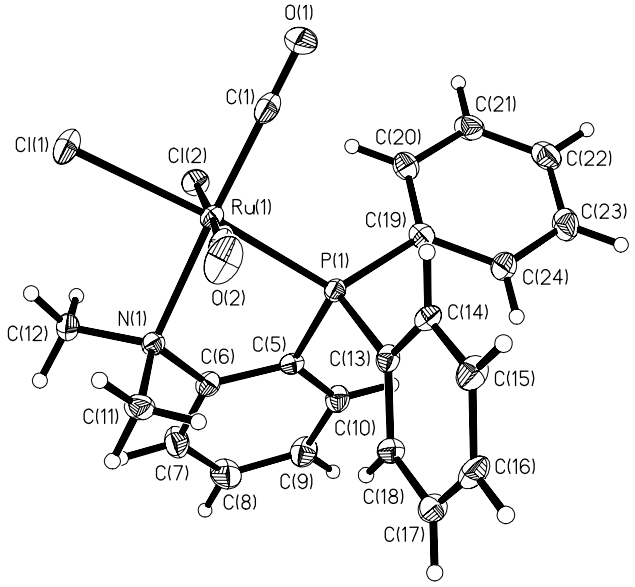

Fig. 2. Molecular structure of (OC-6-42) [$RuCl_2(CO)_2(\eta^2$-np)] (**1**). Thermal ellipsoids are drawn at the 50% probability level.

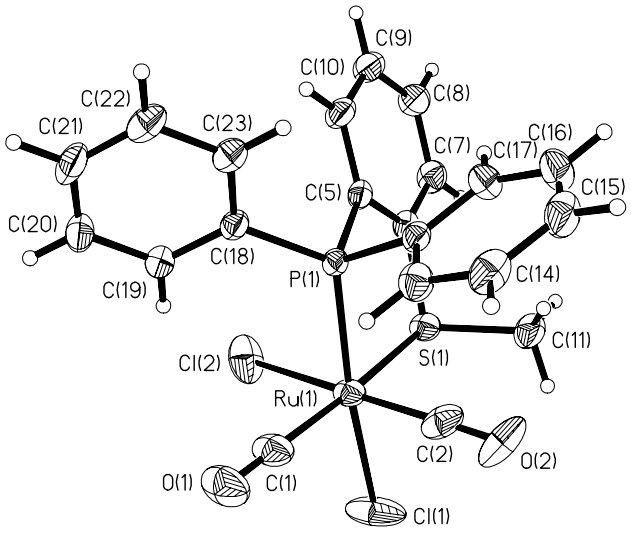

Fig. 3. Molecular structure of (OC-6-43)[$RuCl_2(CO)_2(\eta^2$-sp)] (**2**). Thermal ellipsoids are drawn at the 50% probability level.

tuted phosphanes containing nitrogen in the *ortho* position is that when the chelate is formed is hard to break so the hemilability of these phosphanes is rather limited. The differences in the behaviour of these phosphanes, as well as ours, can be attributed to the basicity of the nitrogen-containing fragment. In the case of pyridine and imidazol both are basic fragments that can interact with the ruthenium centre and coordinate. The ruthenium–nitrogen bond can be cleaved with the help of steric stress introduced by the imidazol or pyridine ring. In our case, the dimethyl amine fragment is highly basic and coordinates too strongly because the electron pair involved in the bond is not delocalized as in the case of pyridine or imidazol.

The (sp) complex of ruthenium (**2**, Fig. 3) shows already somewhat higher reactivity than the (np) complex, producing alcohols to a small extent. In other respects, the behaviour of this ligand is quite similar to the (np). However, the (sp) complex is expected to be slightly less stable than (np), judging from the catalysis results. In most cases, the (sp) forms chelated complexes where the phosphine is coordinated through the phosphorus and sulphur atoms. Examples of non-chelated complexes are rare, but they are known [39]. Our (np) and (sp) ligands have very similar coordination behaviour. They both yield exclusively chelated complexes. However, there are also differences. In the case of (np) basicity of the amino group is key to the interaction with the metal while in the case of (sp) the basic character is much less pronounced. Reports

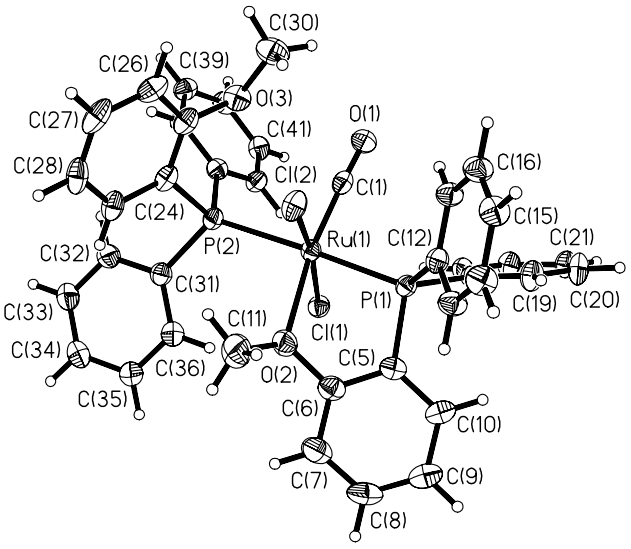

Fig. 4. Molecular structure of (OC-6-12)[$RuCl_2(CO)(\eta^2$-op)(op)] (**3**). Thermal ellipsoids are drawn at the 50% probability level.

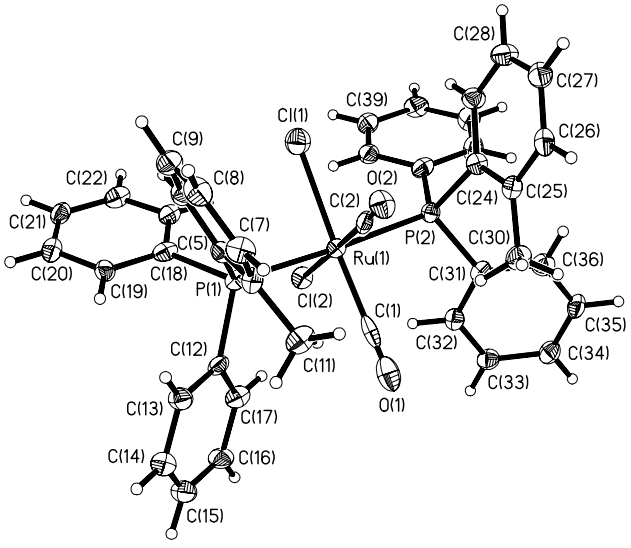

Fig. 5. Molecular structure of (OC-6-33)[$RuCl_2(CO)_2(mep)_2$] (**6**). Thermal ellipsoids are drawn at the 50% probability level. The principle-numbering scheme for **4** and **6**, **8** is similar. Figures of these molecules are supplied as Supplementary material.

in the literature regarding the basicity of aryl-substituted phosphanes suggest that the amino phosphane is more basic ($pK_a = 8.65$) than for example a methoxy phosphane ($pK_a = 4.57$) [40,41]. It can be expected that the methoxy phosphane resembles the thiomethoxy phosphane and thus assume that aminophosphane is also more basic than thiomethoxy phosphane. Recent studies on ring closure kinetics of bidentate hemilabile (np) and (sp) ligands on platinum [42] showed that the ring closure rate constant is faster than the rate constant for the opening, suggesting that the equilibrium between chelated and non-chelated complexes is shifted

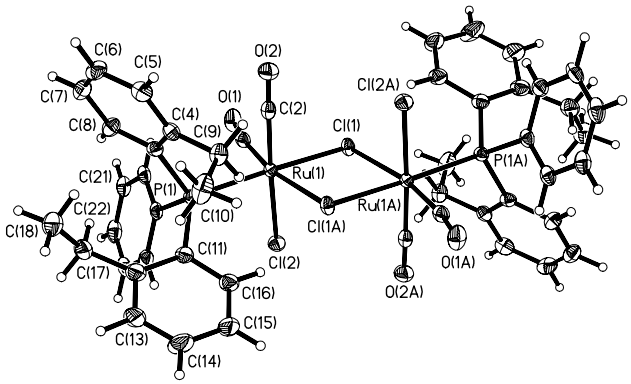

Fig. 6. Molecular structure of $[Ru(\mu\text{-}Cl)Cl(CO)_2(detp)]_2$ (**9**). Thermal ellipsoids are drawn at the 50% probability level. The atom labels "A" indicates atoms at equivalent position $(1 - x, 2 - y, 1 - z)$.

towards the chelated species. This means that once the ring is formed (fast rate) cleavage of the metal–nitrogen or metal–sulphur bond is difficult (slow rate). Furthermore, the study shows that the rate constants are strongly dependent on the nucleophillicity of the linking atom, in our case the nitrogen in (np) is more nucleophillic than the sulphur in (sp). These results provide a ground on which our (np) and (sp) complexes can be compared based on a kinetic parameter.

Among the chelated complexes, the (op) complex **3** displays the best activity. However, complex **3** (Fig. 4) is very unstable and tends to be converted into **4** [24]. This suggests that the catalytic mechanism is not the same as in the case of Ru–(sp) and Ru–(np), and that the structural rearrangement may play an important role during the formation of the catalytic active species. Although the (op) ligand has chelating capabilities like (sp) and (np), it did not chelate under the used experimental conditions. Instead, the obtained main product was the bis phosphane complex **4**. Chelated Ru–(op) complexes have been previously reported in the literature [43,44]. However, the preparation method typically requires the use of higher temperatures, and the syntheses are most commonly carried out under reflux. In the case of our experiment, room temperature reactions resulted solely in the non-chelated complex.

Charge donation seems to have an effect on the strength of the heteroatom-ruthenium bond, in the chelated complexes. In the case of (np), both methyl groups attached to the nitrogen donate charge, making the nitrogen electron pair more willing to interact with the metal. In the (sp) and (op) complexes **2** and **3**, respectively, there is only one methyl group involved. However, the covalent radii of sulphur is larger (1.02 Å) than the radii of oxygen (0.73 Å) [45]. Thus, an effective overlap of the sulphur's p-orbitals with the ruthenium's d-orbitals is possible, making the ruthenium–sulphur interaction stronger than in the case of ruthenium-oxygen.

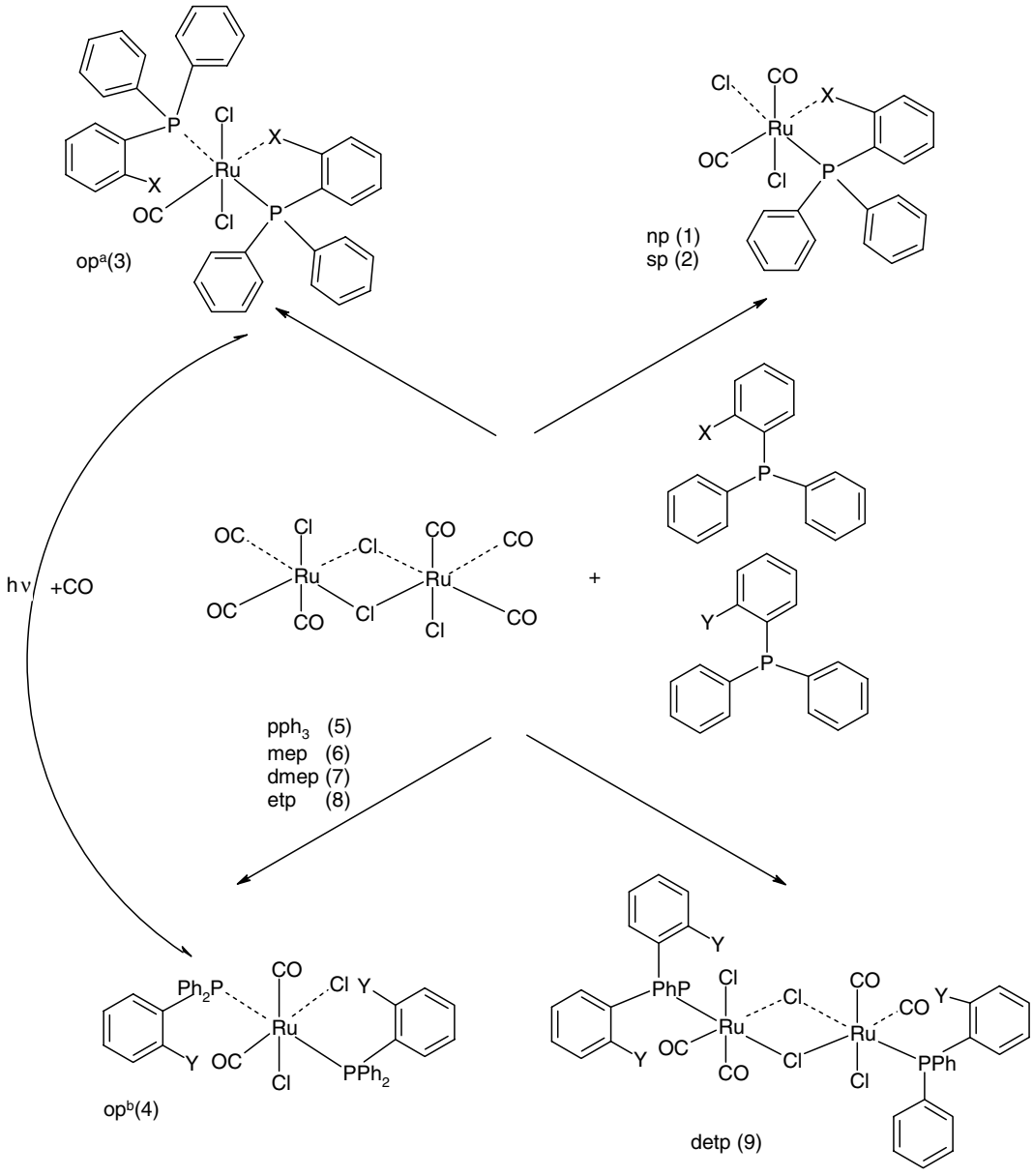

Scheme 1. General reaction products observed during the reaction of $[RuCl_2(CO)_3]_2$ and X = chelating phosphanes; Y = non-chelating phosphanes. $(op)^a$ = chelated complex, $(op)^b$ = non-chelated complex. Reversibility was observed only with the (op) ligand.

For the catalytic process to take place is essential that the precursor is activated. In the case of the chelated complexes we calculated the energy required for the breakdown of the chelate ring and coordination of carbon monoxide (see Scheme 2, for example). Our results show that, in the case of (np) complex **1**, the energy requirements (3 kJ/mol) are low, and in principle the chelate breakdown is possible. However, the lack of reactivity in this complex suggests that the process is not favourable. For the (sp) complex **2**, the energy needed for the chelate to break down (−41 kJ/mol) is more favourable than in the case of (np). This result is consistent with the experimental results, since the complex shows some activity. In the case of (op) complex **3**, cleavage of the chelate is highly favoured and was observed experimentally when the complex rearranged to form **4**. This rearrangement proceeds in solution. When the complex **4** irradiated with UV light in a closed vessel, the product obtained was **3** [24]. However, once the irradiation was stopped, the complex started to re-coordinate CO to form complex **4** (see Scheme 2). The product observed after re-coordination of CO was the cis isomer $(OC\text{-}6\text{-}33)[RuCl_2(CO)_2(op)_2]$ suggesting that the five-coordinate intermediate isomerises from trans to cis before the CO coordinates. This fluxional behaviour of the (op) ligand has been the subject of intense study and several reports in the literature mention the facile cleavage of the ruthenium–oxygen bond by CO [46–49].

Table 3
Catalytic activity for the hydroformylation of 1-hexene

Catalyst	Hydroformylation yield[a] (%)	1-Hexene (%)	Isomers[b]	2-Me-hexanal (%)	1-Heptanal (%)	Total aldehydes (%)	n:i ratio	2-Me-hexanol (%)	1-Heptanol (%)	Total alcohols (%)	n:i ratio
Chelated complexes											
$[RuCl_2(CO)_2(\eta^2\text{-np})]$ (**1**)	0	100	0	0	0	0	–	0	0	0	–
$[RuCl_2(CO)_2(\eta^2\text{-sp})]$ (**2**)	13	56	31	4	5	9	1.5	0	4	4	–
$[RuCl_2(CO)(\eta^2\text{-op})(op)]$ (**3**)	20	62	18	0	4	4	–	6	10	16	1.6
Non-chelated complexes											
$[RuCl_2(CO)_2(op)_2]$ (**4**)	24	33	43	5	8	13	1.8	4	7	11	1.5
$[RuCl_2(CO)_2(pph_3)_2]$ (**5**)	36	6	58	0	9	9	–	7	20	27	3.1
$[RuCl_2(CO)_2(mep)_2]$ (**6**)	55	24	21	0	0	0	–	15	40	55	2.6
$[RuCl_2(CO)_2(etp)_2]$ (**8**)	58	20	22	0	0	0	–	20	38	58	1.9
$[Ru(\mu\text{-Cl})Cl(CO)_2(detp)]_2$ (**9**)	72	7	21	0	4	4	–	29	40	68	1.3
$[RuCl_2(CO)_2(dmep)_2]$ (**7**)	78	6	16	0	21	21	–	16	41	57	2.6

Conditions: T = 130 °C; reaction time = 17 h; n(Ru) = 0.08 mmol; V(solvent) = 5 ml 1-methyl-2-pyrrolidone; V(1-hexene) = 0.5 ml; V(standard) = 0.2 ml cyclohexane; P CO/H_2 1:1: 20 bar.
[a] Alcohols (%) + aldehydes (%).
[b] 2-Hexene and 3-hexene.

The fluxional behaviour has direct implications over the catalytic mechanism. The chelates can break down by carbon monoxide coordination, generating monomers that can then follow a dissociative reaction mechanism, such as the detachment of one phosphane to create a vacancy for coordination. However, fluxional behaviour is restricted to the (op) complex. Thus, chelate breakdown results in the generation of a more reactive species. The (sp) complex **2** shows no obvious fluxional behaviour and as discussed above ring opening in this compound is very slow resulting in a low concentration of active complex in solution. Finally, the inert behaviour of the (np) complex **1** is indicative of its inability to react. As a consequence, cleavage of the ruthenium–heteroatom bond by CO follows the order: (op) > (sp) > (np). This is a good indication of the different hemilabile character of these phosphanes.

3.1.2. Non-chelated complexes

The reaction between the ruthenium dimer $[RuCl_2(CO)_3]_2$ and the non-chelating phosphanes (etp), (dmep), and (mep) yielded monomers containing two carbonyls, two chlorides and two phosphanes (complexes **5** and **6**–**8**; see, for example, Fig. 5). We also prepared the non-chelated (op) complex **4**. This particular complex has been reported previously involving the carbonylation of the bis-chelated complex $[RuCl_2(op)_2]$ [24]. Herein, we report a simple one step synthesis for this complex at room temperature, affording high yields and purity.

When the reaction was performed using the bis[2-(ethyl)phenyl]-(phenyl) phosphane (detp) the unexpected dimer $[RuCl_2(CO)_2(detp)]_2$ **9** was obtained (see Fig. 6). Since this was the only example of such a product among the non-chelated complexes, we examined its mechanism of formation in more detail using DFT methods. The most probable reaction routes to complex **9** from the reaction of $[RuCl_2(CO)_3]_2$ and the (detp) ligand are illustrated in Eqs. ((1)–(4) according to the computational results. Complexes A and B are the proposed intermediates, which have not been isolated.

$$[RuCl_2(CO)_3]_2 + 2(detp) \xrightarrow{-14.3\ kJ/mol} 2[RuCl_2(CO)_3(detp)]\ (\mathbf{A}) \quad (1)$$

$$[RuCl_2(CO)_3(detp)]\ (\mathbf{A}) + (dept) \xrightarrow{34.1\ kJ/mol} [RuCl_2(CO)_2(detp)_2]\ (\mathbf{B}) + CO \quad (2)$$

$$2[RuCl_2(CO)_2(detp)_2]\ (\mathbf{B}) \xrightarrow{-29.2\ kJ/mol} [Ru(\mu\text{-Cl})(Cl)(CO)_2(detp)]_2\ (\mathbf{9}) + 2(detp) \quad (3)$$

$$2[RuCl_2(CO)_3(detp)_2]\ (\mathbf{A}) \xrightarrow{38.2\ kJ/mol} [Ru(\mu\text{-Cl})(Cl)(CO)_2(detp)]_2\ (\mathbf{9}) + 2(CO) \quad (4)$$

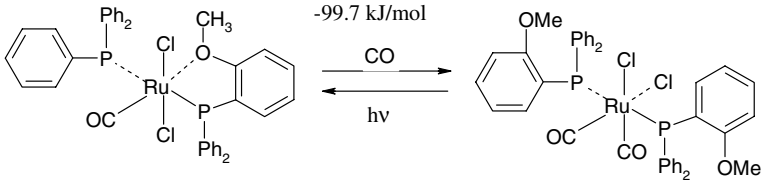

Scheme 2. Rupture of the chelate and rearrangement of (OC-6-12)[$RuCl_2(CO)(\eta^2$-op)(op)].

In order to obtain experimental support for the sequence proposed, we performed the synthesis step by step. In step 1 (Eq. (1)), stoichiometric amounts of ruthenium and phosphane were dissolved separately in ethanol, the solutions were mixed and allowed to react, and the reaction was monitored by IR. After 4 h reaction the tricarbonyl complex (**A** in Eq. (1)) was identified by FT-IR (ν(CO) = 1999s, 2062s (broad), 2135s cm^{-1} in EtOH). In the second step, an excess of phosphane was added and the solution was heated under reflux for 2 h. A gas sample taken from the reaction vessel revealed clearly the release of carbon monoxide (ν(CO) = 2143 cm^{-1}, with typical CO fine structure). Furthermore, the FT-IR of the solution (signals at 2009s, 2071s cm^{-1} in EtOH) confirmed the loss of a carbonyl from the tricarbonyl complex **A** (Eq. (1)). The new dicarbonyl pattern can be related to **C** (Eqs. (3) and (4)).

The energies required to form the dicarbonyl monomer (Eq. (2)) and dicarbonyl dimer (Eq. (4)) are very similar, and they both involve release of carbon monoxide. The formation of the dimer via the dicarbonyl monomer **B** (Eq. (3)) was considered because most of the non-chelating phosphanes form monomers of this type. However, direct formation of the dimer from the tricarbonyl monomer (Eq. (4)) is also possible and requires approximately the same amount of energy as the reaction in Eq. (2). When the solution was kept under reflux for another 4 h, a clear orange-yellow precipitate of **C** was obtained. FT-IR of the solid revealed the same carbonyl signals at 2009s and 2071s cm^{-1} in CH_2Cl_2. Elemental analysis of the solid and ^{31}P NMR confirmed that the product was $[Ru(\mu\text{-}Cl)Cl(CO)_2(detp)]_2$. Although halide-bridged dimers containing small phosphines have been previously reported [38,50–53] examples of ruthenium carbonyl halide-bridged dimers containing bulky phosphanes are less common [54–56].

In 1-hexene hydroformylation, the activities of the complexes containing alkyl-substituted phosphanes were, in general, higher than the activity of unsusbstituted triphenylphosphane. The alkyl-substituted phosphanes are selective towards the production of alcohols. In all of the cases the terminal alcohol was the main product. Alcohols are the result of further hydrogenation of the aldehydes produced, showing that the catalyst operates by means of two different mechanisms. All of the ruthenium complexes with alkyl-substituted phosphanes were monomers (see Fig. 5, for example) except the one with bis, detp = bis[2-(ethyl)-phenyl]-(phenyl) phosphane which is a dimer **9**. In order to study the catalytic activation process in more detail, we modelled the classical generation of a vacancy on the ruthenium centre by assuming a dissociative mechanism for both the monomers and the dimer. The results indicate that the detachment of a phosphane ligand from the monomer is, as expected the most probable initiation step (see Scheme 3). The reaction energy for this step is 53 kJ/mol, while the release of carbonyl would require 180 kJ/mol. This is due to the steric requirement introduced by substitution in the *ortho* position in the phosphane ligand. Experimental evidence of such detachment was observed when the ^{31}P NMR experiments showed free phosphane in solution after catalysis except in the case of the $[Ru(\mu\text{-}Cl)Cl(CO)_2(detp)]_2$ dimer.

With the dimer the process goes along through a different route. We have modelled the generation of a vacancy via cleavage of the chlorine bridge using DFT methods. This route was suggested because the chlorine bridge is known to break readily in the presence of

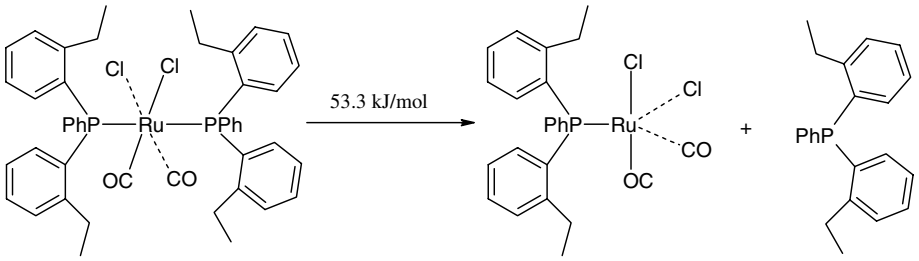

Scheme 3. Generation of a vacancy in a monomeric phosphane-containing complex.

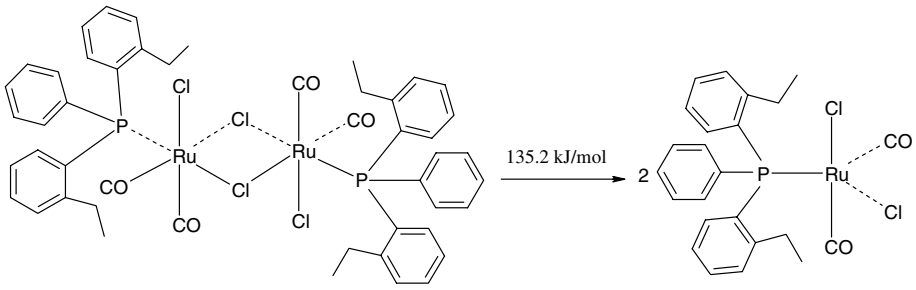

Scheme 4. Cleavage of the dimer and generation of a vacancy.

coordinating solvents [57–59]. The energy requirements for such a cleavage are higher in comparison with the detachment of the phosphane ligand in a monomer (see Scheme 4). However, the dimer is highly active, and cleavage of the chlorine bridge generates monomers with a vacancy for coordination. Furthermore, no evidence of release of phosphane was observed when ^{31}P NMR experiments were performed on the catalytic solution suggesting that detachment of the phosphane in the dimer is unlikely to be the way in which the dimer activates.

3.2. Steric effects

The possible steric effect introduced by the phosphane ligands on the coordinated complexes was estimated by calculating the Tolman cone angles (Table 4). The cone angles were calculated from both experimentally determined crystal structures and from DFT optimized structures. The differences between the cone angles calculated from the X-ray structures and from the optimized structures can be attributed to the packing effects in the crystals. According to the Tolman definition, a wider cone introduces more steric limitations. Most of the chelated phosphanes display lower values for the cone angle. This means less steric stress, and hence more stable complexes. Again, this is in accordance with the observed catalytic activity (Table 3).

Table 4
Calculated cone angles for the coordinated complexes

Catalyst	Calculated cone angle, θ (°)	
	X-ray structure	Computationally optimized structures
$[RuCl_2(CO)_2(\eta^2\text{-np})]$	177	176
$[RuCl_2(CO)(\eta^2\text{-op})(op)]$	182[a]–188[b]	182[a]–188[b]
$[RuCl_2(CO)_2(\eta^2\text{-sp})]$	220	174
$[RuCl_2(CO)_2(op)_2]$	189[a]–197[b]	210[a]–230[b]
$[RuCl_2(CO)_2(pph_3)_2]$	204[a]–206[b]	202[a]–205[b]
$[RuCl_2(CO)_2(mep)_2]$	194[a]–196[b]	201[a]–188[b]
$[RuCl_2(CO)_2(etp)_2]$	184[a]–190[b]	202[a]–212[b]
$[Ru(\mu\text{-}Cl)Cl(CO)_2(detp)]_2$	197[a]–197[b]	188[a]–193[b]
$[RuCl_2(CO)_2(dmep)_2]$	192[a]–192[b]	187[a]–190[b]

[a] Phosphane 1.
[b] Phosphane 2 in the complex.

4. Conclusions

The most active catalysts can be obtained by using weakly bound non-chelating phosphanes, since removal of the phosphane is favourable. Similarly, the lowest activities are related to the complexes, which contain strongly bonded chelated phosphanes. This is primarily due to the stabilization effect associated with the formation of the chelate ring. More stable chelated [2-(dimethylamino)phenyl]-(diphenyl) phosphane and [2-(methylthio)phenyl]-(diphenyl) phosphane complexes **1**–**2** are less willing to participate in the catalytic reactions. Even though [2-(methoxy)phenyl]-(diphenyl) phosphane, is able to chelate the oxygen–ruthenium interaction is weaker than the corresponding N–Ru or S–Ru in the cases of [2-(dimethylamino)phenyl]-(diphenyl) phosphane and [2-(methylthio)phenyl]-(diphenyl) phosphane complexes. Thus, [2-(methoxy)phenyl]-(diphenyl) phosphane behaves more like any of the non-chelated phosphines.

The degree of substitution in the ligand has no marked effect on the catalytic performance. Similar catalytic activity was observed with both mono-substituted and di-substituted phosphanes. Activities in the non-chelated series are related to the steric properties of the phosphanes. Electronic effects are irrelevant in the ruthenium complexes containing alkyl-substituted phosphanes when compared to each other. However, activities of the complexes containing substituted phosphanes are higher compared to unsubstituted phosphane. In this case the electronic effects seems to have influence, since the presence of substituents may stabilize the active intermediates. The steric stress induced by the substituents in the *ortho* position may also facilitate detachment. In other words, substitution in the phosphane increases activities but once substituted the effect is not enhanced by increasing the number of substituents in the ligand.

In the chelated series, catalytic activity seems to be related mainly to the difficulties encountered by the chelated complexes to generate a vacancy. Thus, stabilization via chelate effect reduces the concentration of active intermediates in solution. The poor hemilabile character of the (np) and (sp) complexes results in imme-

diate ring closure and the generation of an inactive complex. On the other hand, the fluxionality exhibited by the hemilabile (op) complex proves to be a disadvantage when the catalytic precursor in non-chelated since high temperature promotes chelation.

Acknowledgement

Financial support provided by the Academy of Finland is gratefully acknowledged (M.H.).

Appendix A. Supplementary data

Crystallographic data for the structural analysis has been deposited with Cambridge Crystallographic Data Centre. CCDC-263091 to CCDC-263098 for **1**–**4** and **6**–**9**, respectively, contains the supplementary crystallographic data for this paper. Copies of this information may be obtained free of charge from The Director, CCDC, 12 Union Road, Cambridge CB2 1EZ, UK (fax: +44 1223 336033; e-mail: deposit@ccdc.cam.ac.uk, or http://www.ccdc.cam.ac.uk). Supplementary data associated with this article can be found, in the online version at doi:10.1016/j.jorganchem.2005.05.016.

References

[1] F. Van Gastel, J.F. Corrigan, S. Doherty, N.J. Taylor, A.J. Carty, Inorg. Chem. 31 (1992) 4492–4498.
[2] S.P. Nolan, T.R. Belderrain, R.H. Grubbs, Organometallics 16 (1997) 5569–5571.
[3] A. Beguin, H.C. Böttcher, G. Suss-Fink, B. Walther, J. Chem. Soc., Dalton Trans. (1992) 2133–2134.
[4] S.Y. Kang, T. Yamabe, A. Naka, M. Ishikawa, K. Yoshizawa, Organometallics 21 (2002) 150–160.
[5] M. Kranenburg, P.C. Kamer, P.W. Van Leeuwen, W.N. Piet, Eur. J. Inorg. Chem. 2 (1998) 155–157.
[6] C. Darcel, E.B. Kaloun, R. Merdes, D. Moulin, N. Riegel, S. Thorimbert, J.P. Genet, S. Juge, J. Organomet. Chem. 624 (2001) 333–343.
[7] J. Elek, L. Nadasdi, G. Papp, G. Laurenczy, F. Joo, Appl. Catal. A 255 (2003) 59–67.
[8] X. Dong, C. Erkey, J. Mol. Catal. A 211 (2004) 73–81.
[9] H. Horvath, G. Laurenczy, A. Katho, J. Organomet. Chem. 689 (2004) 1036–1045.
[10] H. Sertchook, D. Avnir, J. Blum, F. Joo, A. Katho, H. Schumann, R. Weimann, S. Wernik, J. Mol. Catal. A 108 (1996) 153–160.
[11] C. Slugovc, E. Ruba, R. Schmid, K. Kirchner, Organometallics 18 (1999) 4230–4233.
[12] R.C. Van der Drift, M. Vailati, E. Bowman, E. Drent, J. Mol. Catal. A 159 (2000) 163–177.
[13] A. Salvini, P. Frediani, F. Piacenti, J. Mol. Catal. A 159 (2000) 185–195.
[14] A. Salvini, F. Piacenti, P. Frediani, A. Devescovi, M. Caporali, J. Organomet. Chem. 625 (2001) 255–267.
[15] P. Smoleñski, F.P. Pruchnik, Z. Ciunik, T. Lis, Inorg. Chem. 42 (2003) 3318–3322.
[16] V.K. Srivastava, R.S. Shukla, H.C. Bajaj, R.V. Jasra, J. Mol. Catal. A 202 (2003) 65–72.
[17] E. Lozano Diz, A. Neels, H. Stoeckli-Evans, G. Suss-Fink, Polyhedron 20 (2001) 2771–2780.
[18] M. Beller, B. Zimmermann, H. Geissler, Chem. Eur. J. 5 (4) (1999) 1301–1305.
[19] C. Schluenken, M.A. Esteruelas, F. Lahoz, L.A. Oro, H. Werner, Eur. J. Inorg. Chem. 12 (2004) 2477–2487.
[20] C.A. Sandoval, T. Ohkuma, K. Muniz, R. Noyori, J. Am. Chem. Soc. 125 (44) (2003) 13490–13503.
[21] C. Beddie, M.B. Hall, J. Am. Chem. Soc. 126 (42) (2004) 13564–13565.
[22] C.W. Rogers, M.O. Wolf, Chem. Commun. (1999) 2297–2298.
[23] M.S. Khoshbin, M.V. Ovchinnikov, C.A. Mirkin, L.N. Zakharov, A.L. Rheingold, Inorg. Chem. 44 (2005) 496–501.
[24] J.C. Jeffrey, T.B. Rauchfuss, Inorg. Chem. 18 (10) (1979) 2658–2666.
[25] A.A. Batista, J. Zuckerman-Schpector, O.M. Porcu, S.L. Queiroz, M.P. Araujo, G. Oliva, D.H.F. Souza, Polyhedron 13 (1994) 689–691.
[26] Z. Otwinowski, W. Minor, in: C.W. CarterJr., R.M. Sweet (Eds.), Processing of X-ray Diffraction Data Collected in Oscillation Mode, Methods I Enzimology, Macromolecular Crystallography, Part A, vol. 276, Academic Press, New York, 1997, pp. 307–326.
[27] G.M. Sheldrick, SHELXS-97: Program for Crystal Structure Determination, University of Göttingen, Göttingen, Germany, 1997.
[28] M.C. Burla, M. Camalli, B. Carrozzini, G.L. Cascarano, C. Giacovazzo, G. Polidori, R. Spagna, SHELXTL 6.14, J. Appl. Crystallogr. 36 (2003) 1103.
[29] G.M. Sheldrick, SHELXTL V. 6.14, Bruker Analytical X-ray Systems, Bruker AXS, Inc., Madison, WI, USA, 2003.
[30] G.M. Sheldrick, SHELXL-97: Program for Crystal Structure Refinement, University of Göttingen, Göttingen, Germany, 1997.
[31] L.J. Farrugia, J. Appl. Crystallogr. 32 (1999) 837.
[32] S. Huzinaga (Ed.), Gaussian Basis Sets for Molecular Calculations Physical Sciences Data 16, Elsevier, Amsterdam, 1984.
[33] E.S. Chandrika, S. Ma, S.J. Rettig, B.R. James, W.R. Cullen, Inorg. Chem. 36 (1997) 5426–5427.
[34] C.B. Pamplin, E.S. Ma, N. Safari, S.J. Rettig, B.R. James, J. Am. Chem. Soc. 123 (2001) 8596–8597.
[35] I. Moldes, E. Encarnacion, J. Ros, A. Alvarez-Larena, J.F. Piniella, J. Organomet. Chem. 566 (1998) 165–174.
[36] A. Dervisi, P.G. Edwards, P.D. Newman, R.P. Tooze, S.I. Coles, M.B. Hursthouse, J. Chem. Soc., Dalton Trans. (1998) 3771–3776.
[37] A. Dervisi, P.G. Edwards, P.D. Newman, R.P. Tooze, J. Chem. Soc., Dalton Trans. (2000) 523–528.
[38] A. Caballero, F.A. Jalon, B.R. Manzano, G. Espino, M. Perez-Manrique, A. Mucientes, F.J. Poblete, M. Maestro, Organometallics 23 (2004) 5694–5706.
[39] L. Hirsivaara, M. Haukka, S. Jaaskelainen, R. Laitinen, E. Niskanen, T.A. Pakkanen, J. Pursiainen, J. Organomet. Chem. 579 (1–2) (1999) 45–52.
[40] C.A. Streuli, Anal. Chem. 32 (1960) 985–987.
[41] T. Allman, R.G. Goel, Can. J. Chem. 60 (6) (1982) 716–722.
[42] R. Romeo, L. Monsu-Scolaro, M.R. Plutino, A. Romeo, F. Nicolo, A. Del Zotto, Eur. J. Inorg. Chem. (2002) 629–638.
[43] C.W. Roggers, B.O. Patrick, S.J. Rettig, M.O. Wolf, J. Chem. Soc., Dalton Trans. (2001) 1278–1283.
[44] Y. Yamamoto, K.-I. Sugawara, T. Aiko, J.-F. Ma, J. Chem. Soc., Dalton Trans. (1999) 4003–4008.
[45] J.E. Huheey, E.A. Keiter, R.L. Keiter, in: Jane Piro (Ed.), Inorganic Chemistry, fourth ed., HarperCollins College Publishers, New York, 1993, p. 253 (Chapter 8).
[46] E. Benedetti, G. Braca, G. Sbrana, F. Salvetti, B. Grassi, J. Organomet. Chem. 37 (1972) 361–373.
[47] M.I. Bruce, F.G.A. Stone, J. Chem. Soc. A (1967) 1238.

[48] P. Braunstein, D. Matt, Y. Dusausoyz, Inorg. Chem. 22 (1983) 2043–2047.
[49] P. Braunstein, D. Matt, D. Nobel, S.-E. Bouaoud, B. Carluer, D. Grandejan-Lemoine, J. Chem. Soc., Dalton Trans. (1986) 415.
[50] B. deKlerk-Engels, J.H. Groen, K. Vrieze, A. Mockel, E. Lindner, Inorg. Chim. Acta 195 (1992) 237.
[51] E. Lindaer, A. Mikkel, M. Steimann, H. Kiihbauch, R. Fawzi, H.A. Mayer, Inorg. Chem. 32 (1993) 1266–1271.
[52] T.G. Southern, P.H. Dixneuf, J.-Y. Le Marquille, D. Grandjean, Inorg. Chem. 18 (11) (1979) 298.
[53] R. Sanchez-Delgado, M. Medina, F. Lopez-Linares, A. Fuentes, J. Mol. Catal. A 116 (1997) 167–177.
[54] A.V. Marchenko, J.C. Huffman, P. Valerga, M. Jimenez-Tenorio, M.C. Puerta, K.G. Caulton, Inorg. Chem. 40 (2001) 6444–6450.
[55] M-K. Chung, G. Ferguson, V. Robertson, M. Shalf, Can. J. Chem. 79 (2001) 949.
[56] T. Gottschalk-Gaudig, K. Folting, K.G. Caulton, Inorg. Chem. 38 (1999) 5241–5245.
[57] S.D. Drouin, D. Amoroso, G.P.A. Yap, D.E. Fogg, Organometallics 21 (2002) 1042–1049.
[58] V. Cadierno, P. Crochet, J. Dez, S.E. Garca-Garrido, J. Gimeno, Organometallics 22 (2003) 5226–5234.
[59] B.F.G. Johnson, R.D. Johnston, J. Lewis, J. Chem. Soc. A (1969) 792–796.